ENVIRONMENTAL STUDIES

Artificial lake expansion amplifies mercury pollution from gold mining

Jacqueline R. Gerson[1]*†, Simon N. Topp[2]*†, Claudia M. Vega[3,4], John R. Gardner[2], Xiao Yang[2], Luis E. Fernandez[3,4,5], Emily S. Bernhardt[1], Tamlin M. Pavelsky[2]

Artisanal and small-scale gold mining (ASGM) is the largest global source of anthropogenic mercury emissions. However, little is known about how effectively mercury released from ASGM is converted into the bioavailable form of methylmercury in ASGM-altered landscapes. Through examination of ASGM-impacted river basins in Peru, we show that lake area in heavily mined watersheds has increased by 670% between 1985 and 2018 and that lakes in this area convert mercury into methylmercury at net rates five to seven times greater than rivers. These results suggest that synergistic increases in lake area and mercury loading associated with ASGM are substantially increasing exposure risk for people and wildlife. Similarly, marked increases in lake area in other ASGM hot spots suggest that "hydroscape" (hydrological landscape) alteration is an important and previously unrecognized component of mercury risk from ASGM.

INTRODUCTION

Informal—mostly illegal—artisanal and small-scale gold mining (ASGM) is the primary contributor to global atmospheric mercury (Hg) pollution (*1*) and an important driver of deforestation (*2*–*4*), sediment loading (*5*, *6*), and biodiversity loss (*7*–*9*) across the Global South. Simultaneously, ASGM provides livelihoods for tens of millions of people (*10*) across over 70 countries worldwide (*11*). Within the Madre de Dios region of the Peruvian Amazon—a global biodiversity hot spot and home to numerous indigenous communities—ASGM has been responsible for the deforestation of nearly 14% (~95,000 ha) of the landscape between 1984 and 2017 (*4*) and is estimated to release approximately 180 metric tons of Hg annually, according to a recent report by the Artisanal Gold Council (*12*).

During ASGM, gold-laden sediments from rivers, oxbow lakes, and floodplains are processed through a combination of sluicing and settlement ponds in which elemental Hg is added to isolate the gold. The Hg within this Hg-gold amalgam is then burned off and released into the atmosphere, while Hg-enriched tailings are dumped into nearby aquatic ecosystems. Once methylated by microbes, predominantly under anoxic conditions, methylmercury (MeHg) bioaccumulates and biomagnifies across the food web (*13*), leading to neurotoxic impacts in terrestrial and aquatic biota (*14*, *15*) and people (*16*). In addition to deforestation and Hg loading, ASGM alters the landscape by creating thousands of small mining ponds (Fig. 1), which, in turn, can cause site-specific externalities, such as increased malaria transmission (*17*, *18*) and contamination of agricultural land (*19*). The size and connectivity of these ponds vary, but their presence is ubiquitous and has implications for the processing and bioavailability of Hg.

In this study, we sought to understand how ASGM changes the extent of lotic (riverine) and lentic (lake) environments and how Hg loading and net methylation differ across these environments. We analyzed remote sensing data of the Madre de Dios region over the past 34 years to quantify changing areas of lotic and lentic systems and to understand how mining alters the landscape to create environments suitable for Hg methylation. We also collected unfiltered water (representing the summation of the dissolved and suspended fractions) and bulk sediment samples from a 200-km reach of the Madre de Dios River, its tributaries, and surrounding oxbow lakes and mining ponds. Sampling occurred in areas both upstream and downstream of ASGM activity to test its impact on the transport and fate of Hg. In each sample, we measured concentrations of total Hg and MeHg. We use MeHg concentrations as indicative of net Hg methylation, which represents both methylation and demethylation processes. Of the eight watersheds included in the study, mining operations have largely occurred in the Colorado and Inambari watersheds (*3*, *4*). Three watersheds are located downstream of these

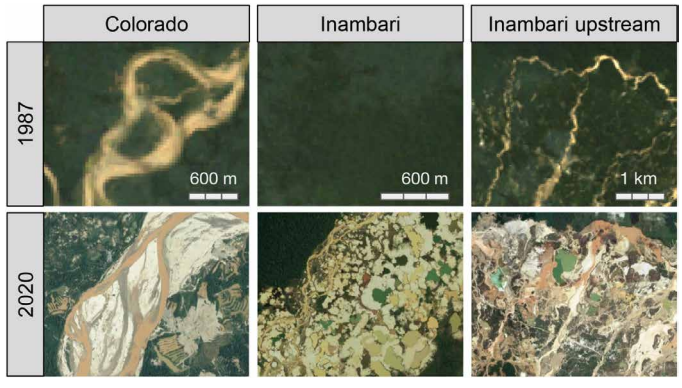

Fig. 1. Comparison of historical (1987; Landsat) and current [2020; Google Earth from Maxar, Airbus, and Centre National d'Etudes Spatiales (CNES)] landcover for mining-affected locations. Locations along the Colorado River (left), adjacent to the Inambari River (middle), and in the Inambari headwaters (right) show the proliferation of mining ponds and deforestation. Specific locations can be seen in fig. S1. Top and bottom panels cover the same spatial extent. Note that in 1987, the Inambari area shown contained 100% forest cover.

[1]Department of Biology, Duke University, Durham, NC 27708, USA. [2]Department of Geological Sciences, University of North Carolina–Chapel Hill, Chapel Hill, NC 27599, USA. [3]Centro de Innovación Científica Amazónica (CINCIA), Puerto Maldonado, Madre de Dios, Peru. [4]Center for Energy, Environment and Sustainability (CEES), Wake Forest University, Winston-Salem, NC 27109, USA. [5]Department of Global Ecology, Carnegie Institution for Science, Stanford, CA 94305, USA.
*These authors contributed equally to this work and are co-first authors.
†Corresponding author. Email: jgerson1@gmail.com (J.R.G.); sntopp@live.unc.edu (S.N.T.)

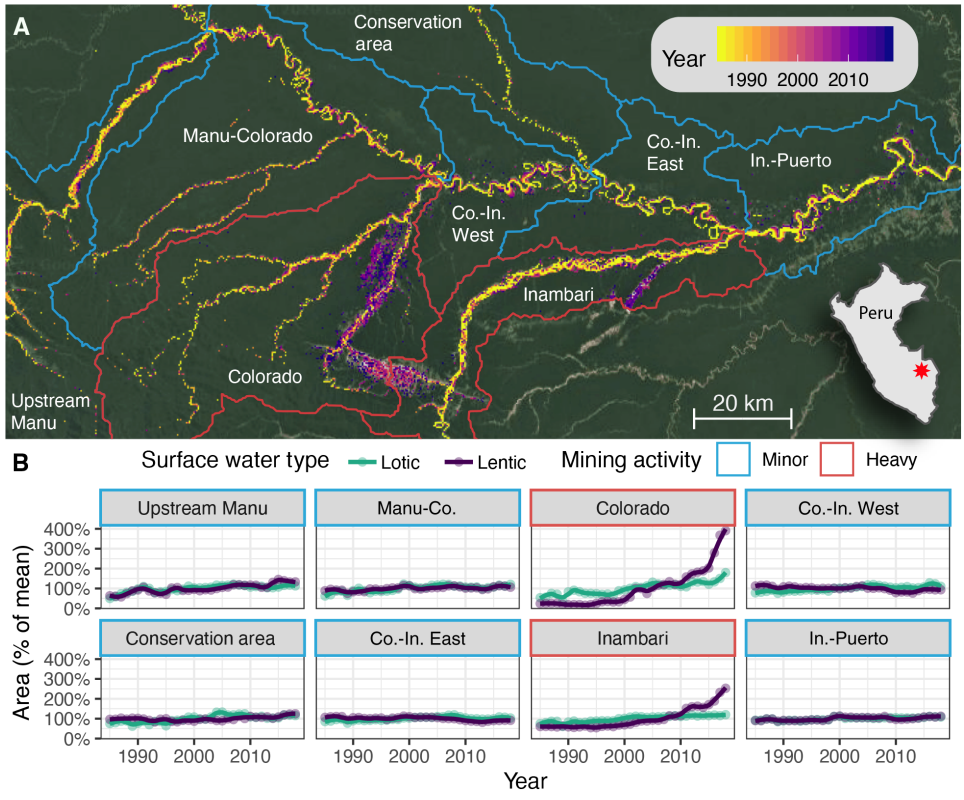

Fig. 2. Spatial and temporal distribution of surface water extents in Madre de Dios, Peru. (**A**) Map of the study area with historical surface water extent. Colors represent the first year a given area was detected as water. Historic river channels that predate satellite observations appear in yellow, while recent morphological changes and the expanse in mining ponds appear in magenta. (**B**) Time series of normalized surface water extent broken down by watershed and lentic versus lotic environments. All water pixels connected to the main river channel for a given year are considered lotic; water pixels isolated from the main river channel are considered lentic. Base map imagery from Google Earth (2020, from Landsat/Copernicus). See https://sntopp.users.earthengine.app/view/mdd-hydroscape-explorer for enhanced visualization of hydroscape changes. Sampling locations for mercury analysis are shown in fig. S1.

two heavily mined watersheds (Co.-In. West, Co.-In. East, and In.-Puerto), and three watersheds are located upstream (Upstream Manu, Reserve, and Manu-Co.; Fig. 2).

RESULTS

Changes to the hydroscape

Our results highlight the "lentification" (increased extent of slow-moving pond and lake ecosystems) of the Madre de Dios region that accompanies extensive ASGM activities, with lentic systems increasing by an average of 16 km^2 (670%) in heavily mined watersheds from the period 1985–1989 to 2014–2018, compared to only 0.83 km^2 (20%) in less affected areas. Although we found that between 1985 and 2018, both lotic (all eight watersheds) and lentic systems (six of eight watersheds) increased overall in surface water extent ($P < 0.0001$), these changes vary by orders of magnitude between watersheds with and without extensive ASGM activity. In heavily mined watersheds, average surface extent of lakes and rivers over the 34 years increased by 0.53 km^2 $year^{-1}$ (6.63% $year^{-1}$) and 1.22 km^2 $year^{-1}$ (2.13% $year^{-1}$), respectively. Comparatively, in less heavily mined watersheds, the average change in lake area was roughly 16 times smaller (0.02 km^2 $year^{-1}$, 0.41% $year^{-1}$), and the rate of change in river surface area was substantially lower (0.39 km^2 $year^{-1}$, 1.06% $year^{-1}$). Most of this increase in lake surface area was due to the proliferation of mining ponds after the year 2000 (Fig. 2). This result parallels documented increases in ASGM activity, which were generally low from 1984 to 2000 and began to rise rapidly thereafter, with the largest increases following the 2008 global economic recession, and remaining consistently high since 2010 (*3*, *4*). The increase in river surface area in mined regions is primarily due to the expanded connectivity between the main channel and adjacent mining operations. These changes are likely similarly driven by ASGM operations on riverbanks. Although water classifications as lotic or lentic near riverbanks change between the two states due to seasonal changes in connectivity, these intra-annual changes are small relative to interannual trends in lentic area throughout the study period.

Previous studies have shown that ASGM leads to extensive deforestation of the landscape (*2*, *4*). To examine the extent of previously forested land that has been converted into aquatic systems, we partitioned deforestation into areas converted to barren ground and areas converted to aquatic systems for the year following the deforestation. We found that 66 km^2 of the 914 km^2 of deforested land in our study area (7.2% of previously forested areas) has been converted directly to lotic or lentic environments, with most of this conversion occurring in areas heavily affected by mining (fig. S2). As deforestation mobilizes soil, it leads to increased sedimentation and Hg transport into surrounding water bodies (*20*), potentially increasing net Hg methylation rates and disproportionately affecting aquatic organisms inhabiting areas directly converted from forested to aquatic landscapes.

Landscape patterns in mercury concentration

We found that mercury loading was highest in river segments containing floodplain mining or downstream of substantial ASGM activity (hereafter referred to as downstream rivers; $P < 0.0001$; Fig. 3). Total Hg concentrations in these river waters were ~10 times that of other water bodies: 10.1 ± 2.8 ng Hg liter^{-1} ($n = 12$; reported as means ± SE), compared with 1.7 ± 0.4 ng Hg liter^{-1} ($n = 12$) in mining ponds and 1.3 ± 0.3 ng Hg liter^{-1} ($n = 10$) in downstream oxbow lakes. Average downstream river water total Hg concentration was 1100 times the total Hg concentration of upstream river water and represented 9 of the 10 samples with the highest water column total Hg concentrations. Similar trends of elevated Hg concentration in rivers downstream of ASGM have previously been reported, including in Peru (*21*, *22*), but this is the first study to our knowledge that concurrently examines Hg trends from ASGM in both lake and river systems.

Given the correlation between total suspended solids (TSSs) and water column total Hg concentration found in this study ($P < 0.0001$, $r^2 = 0.62$; fig. S3) and other studies (*23*–*25*), as well as the higher concentration of TSS in downstream rivers compared with the other measured water bodies ($P < 0.0001$; fig. S4), we expect that Hg is transported bound to sediment particles (i.e., as particulate Hg) rather than in the dissolved fraction. Our finding of higher total Hg concentrations in oxbow lake sediments compared with downstream river sediments ($P = 0.030$; fig. S5) and the higher percent carbon content of oxbow lakes compared with other water bodies ($P < 0.005$) supports this assumption. Given this finding, it is important to note that sampling took place during dry season low-flow conditions. During the wet season (around October to April), precipitation increases three to five times, leading to meter-scale increases in river stage (*26*). While these increased flows historically created a highly seasonal flux of suspended sediment into the river, ASGM-driven erosion during the dry season is inverting historical seasonal patterns of suspended sediment concentrations in heavily mined areas of the watershed (*6*), potentially exacerbating Hg transport and subsequent contamination of downstream aquatic environments.

Although water column total Hg concentrations were highest in downstream rivers, we found that the mining ponds and oxbow lakes were significantly more net efficient in converting Hg to the bioavailable form of MeHg (determined by the percentage of Hg as MeHg; $P = 0.0032$ and $P = 0.0003$, respectively). It is thus a combination of transport processes and residence times that is important for the fate of Hg in this landscape. On average, downstream river water contained 1.1 ± 0.3% of Hg as MeHg ($n = 12$; reported as means ± SE), compared to 5.8 ± 1.2% ($n = 12$) in mining ponds and 7.9 ± 2.1% in downstream oxbow lakes ($n = 10$). Despite different total Hg loadings, downstream rivers, oxbow lakes, and mining ponds contained the same average concentration of MeHg ($P > 0.05$). These trends are likely driven by the biogeochemical factors that promote methylation within lentic systems compared with lotic systems, as oxygen-limited systems generally have higher MeHg production than well-oxygenated systems (*27*, *28*). Note also that water column MeHg concentrations were not significantly correlated

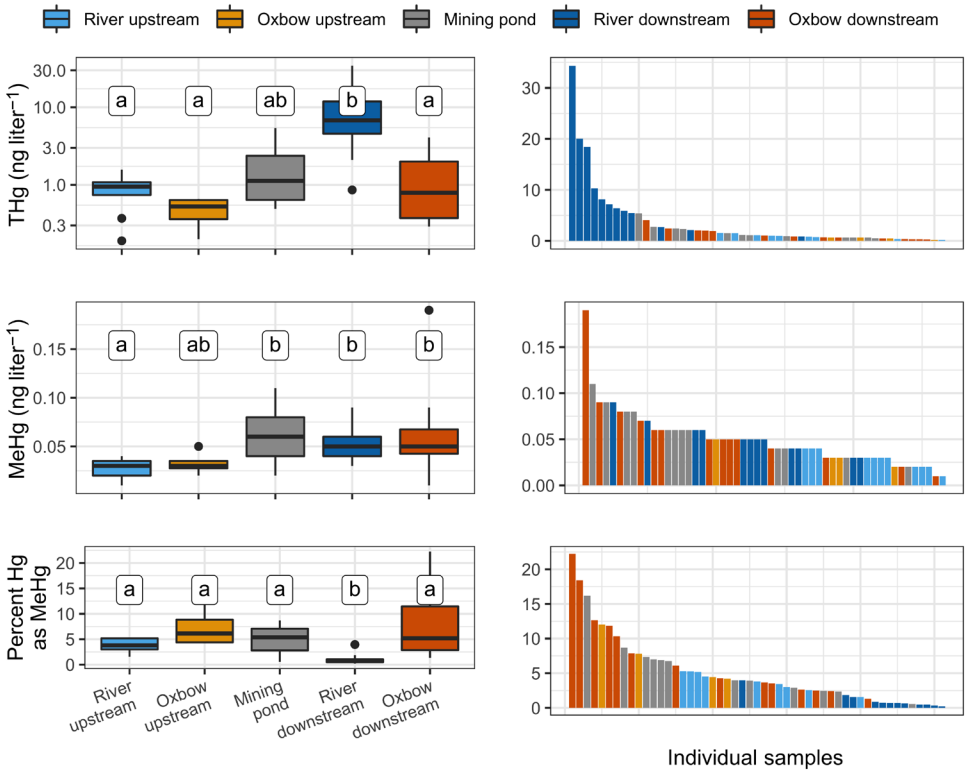

Fig. 3. Concentration and distribution of water column total Hg (THg), methyl Hg (MeHg), and percent Hg as MeHg across water bodies upstream and downstream of artisanal gold mining in Madre de Dios, Peru. Right column distribution data are observations shown in order of decreasing Hg values to highlight clustering among sampling locations. Letters represent statistically significant differences between values at each location according to a Kruskal-Wallis analysis of variance on ranks, followed by Dunn's test.

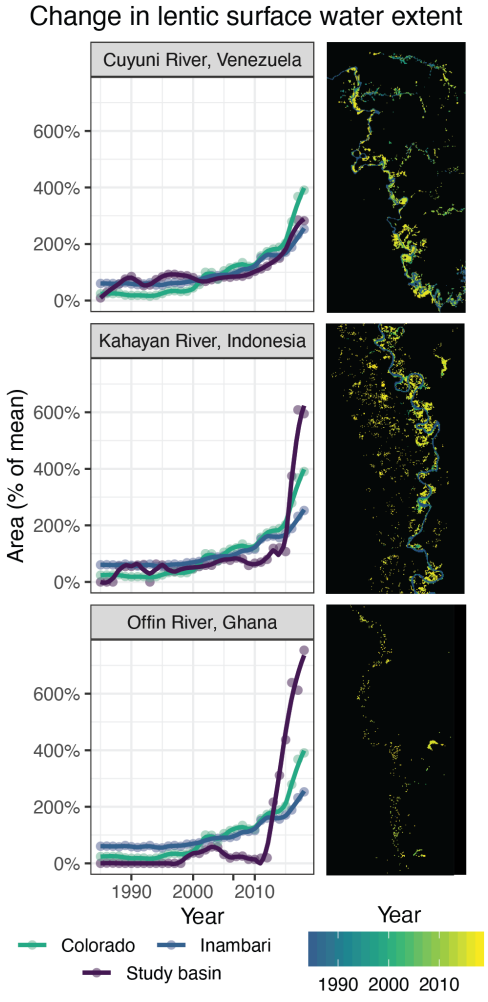

Fig. 4. Global examples of landscape lentification from three countries heavily affected by ASGM. The left column shows the relative lentic surface area of the study country (in purple) compared with the heavily mined basins in Peru. The right column shows the historic water masks of the study country with colors denoting the first year a given pixel was classified as water. The main channel in the Offin River is smaller than 30 m wide and below the remote sensing detection threshold; therefore, only surrounding mining ponds are measured. Black areas in the figures on the right represent pixels classified as land throughout the study period.

with TSS ($P = 0.18$; fig. S3), suggesting that factors other than TSS are driving trends in MeHg. The combined effects of higher net methylation efficiency found in oxbow lakes and ponds and the lentification of the hydroscape are highly likely to be increasing the risk of exposure to MeHg across ASGM-impacted regions beyond what might be anticipated on the basis of the enhanced Hg loading alone.

DISCUSSION

ASGM within the Madre de Dios region of Peru creates a synergistic effect between Hg loading and landscape lentification by expanding the systems that promote methylation of inorganic Hg into MeHg. Between 1985–1989 and 2014–2018, the total surface area of lentic and lotic environments in heavily mined areas has increased by 670 and 98%, respectively. Our results show that net MeHg production is five- to seven-fold greater in lentic than in lotic systems within the study area. In combination, landscape lentification and Hg loading are substantially increasing Hg bioavailability. This trend is likely to continue as long as gold prices remain high and ASGM activities remain a feasible livelihood for local populations living in less regulated areas. Increased Hg bioavailability in this global biodiversity hot spot poses a serious threat to local communities, including recently contacted indigenous groups, that consume high trophic level fish (*29*) and to endangered species such as the iconic Giant Otter (*Pteronura brasiliensis*) that depend on lentic systems for habitat and foraging grounds (*30*).

To our knowledge, this is the first examination of interactions between Hg fate and transport and landscape hydrology associated with ASGM practices. Our results clearly show that the Madre de Dios region is vulnerable to the synergistic effects of lentification and Hg loading. Although this region is of particular concern due to its high levels of biodiversity, it is likely that Hg bioavailability is also increasing in other ASGM hot spots throughout the world. To determine whether this landscape lentification is a pervasive trend associated with ASGM, we examined the changing hydroscape in three additional ASGM hot spots around the globe (Fig. 4). Watersheds with heavy mining activity in Venezuela (*31*), Ghana (*18*), and Indonesia (*32*) have all had three- to eight-fold increases in the extent of lentic environments over the past 34 years. Assuming similar relative net methylation rates as in the Madre de Dios region, the ASGM-associated increase in lentic environments across the globe promotes net Hg methylation and bioaccumulation throughout the food chain. This process increases the threat from ASGM activities to vulnerable communities around the globe while simultaneously leading to severe ecological degradation. Thus, in evaluating the effects of Hg from ASGM, we need to consider not only the overall loading of Hg into the aquatic ecosystem but also how changes in the hydroscape might be influencing the processing of this Hg, particularly in global biodiversity hot spots.

MATERIALS AND METHODS

Sample collection

All samples for Hg analysis were collected in July and August 2019 during the dry season (fig. S1). River samples were collected from the Madre de Dios River mainstem, upstream of a river confluence, downstream of a confluence, and from each tributary. One water sample was taken from near the water surface at each sampling point after the boat motor had been off for at least 1 min. For oxbow lakes and mining ponds, one water sample was taken from the water surface. Water samples were collected using the clean hands–dirty hands protocol [U.S. Environmental Protection Agency (EPA) Method 1669] in new polyethylene terephthalate copolyester glycol bottles and acidified to 0.4% with trace grade hydrochloric acid within 24 hours of collection. Water samples were stored on ice in the field and then stored at 4°C until analysis. Note that all water samples are unfiltered, and all Hg values reported represent the concentration for the total water column. River sediment samples were collected underwater from the channel margins by compositing surficial sediment from at least five sampling points along a 30-m transect using a shovel. These samples were taken during the dry season; during the wet season, the sampling locations are closer to the center of the channel since the width of the river increases by tens of meters. We therefore assume that the river sediment samples we collected are representative of well-mixed fluvial sediments. Oxbow lake and

mining pond sediments were collected as channel margin sediment using a shovel (collected underwater as surficial sediment) and from three points in the center of the lake using an Eckman grab sampler. Sediment samples were collected using the clean hands–dirty hands protocol, double bagged, frozen on dry ice in the field, and stored frozen until sample processing. Note that mining ponds were sampled in the La Pampa region, a watershed located adjacent to the Colorado watershed. La Pampa is an area that, until recently, contained widespread ASGM (*4*). It has been under military control since February 2019 (Operacion Mercurio), making it a safe area for field sampling. Because of logistical and safety concerns stemming from a lack of police or military presence, it was not possible to sample mining ponds from the other actively mined watersheds examined in this study; however, mining practices in La Pampa are representative of those in the region.

Water samples for TSS were collected immediately after collecting water samples for Hg analysis. Water from just below the surface was pumped through a drill-operated pump with in-line glass fiber filter (preweighed), and the amount of water filtered was recorded. The filter was stored frozen until sample processing. A filter field blank was also taken and frozen for analysis.

Laboratory analyses

Unfiltered water samples were analyzed for total Hg via oxidation with bromine chloride for a minimum of 24 hours, purge and trap, cold vapor atomic fluorescence spectroscopy (CVAFS), and gas chromatographic (GC) separation (EPA Method 1631, revision E) on a Tekran 2600 Automated Total Mercury Analyzer. Calibration and continuous calibration verification (CCV) were performed using Brooks Rand Instruments Total Mercury Standard (1.0 ng liter^{-1}), and initial calibration verification was performed using SPEX CentriPrep inductively coupled plasma mass spectrometry (ICP-MS) multielement in solution standard 2A. Instrument detection limit was 0.5 ng liter^{-1}. All standards had average recoveries within 10% of the accepted values. The field blank, digestion blanks, and analysis blanks were below detection limit (BDL).

After lyophilization for at least 5 days, sediment samples were analyzed for total Hg on the Milestone Direct Mercury Analyzer (DMA-80) via thermal decomposition, catalytic reduction, amalgamation, desorption, and atomic absorption spectroscopy (EPA Method 7473). Calibration of the DMA-80 was performed using Brooks Rand Instruments Total Mercury Standard (1.0 ng liter^{-1}). CCV and matrix spike (MS) were performed using the National Institute of Standards and Technology (NIST) standard reference material 1633c (coal fly ash, 1005 ng g^{-1}), and quality control standard (QCS) was performed using NIST-certified reference material 2709a (San Joaquin Soil, 1100 ng g^{-1}). Instrument detection limit was 0.5 ng Hg. All samples were run in duplicate, with values accepted when the relative percent difference between the two samples was within 10%. All standards and MS had average recoveries within 10% of the accepted values, and all blanks were BDL.

For MeHg, unfiltered water samples were extracted with trace grade sulfuric acid for a minimum of 24 hours (*33*). Samples were analyzed by aqueous ethylation with sodium tetraethylborate, purge and trap, CVAFS, GC, and ICP-MS on an Agilent 770 (EPA Method 1630) (*34*, *35*). Calibration and CCV were performed using Brooks Rand Instruments Methylmercury Standard (1 ng liter^{-1}). Method detection limit was 1 pg MeHg. All standards had average recoveries within 13% of the accepted values, and all blanks were BDL.

For TSS, filters were placed in the oven at 105°C for 48 hours. Filters were then reweighed. TSS was defined as the difference in filter mass before and after filtration divided by the volume of water that passed through the filter. The filter field blank had a negligible difference in mass.

Surface water extent analyses

Annual surface water extent for the study area was calculated using the JRC Global Surface Water Mapping Layers v1.1 (*36*) in Google Earth Engine (*37*). This dataset includes global surface water masks at 30-m resolution annually between 1984 and 2018. Because of gaps in the annual water masks caused by cloud cover, areas classified as seasonal and permanent water were overlaid in 2-year intervals starting in 1985. The resulting yearly masks are therefore the maximum extent of surface water from the designated year and the year prior. Although this method may slightly overestimate water surface extent, it remains constant throughout the study, so proportional changes in lentic and lotic systems remain unaffected.

Lentic versus lotic environments were delineated by overlaying the annual surface water masks with the Global River Widths from Landsat (GRWL) database (*38*). GRWL includes centerlines for all rivers wider than 30 m globally. Lotic water pixels located within river channels were identified using cumulative cost mapping with GRWL centerlines as source pixels (*39*). Cumulative cost mapping integrates the "cost" of traversing given pixels out from a source node. By assigning water pixels a cost of 0 and land pixels a cost of 1, it is possible to effectively determine connectivity to the GRWL centerline. Morphological changes over time cause some adjacent ponds and oxbow lakes to sporadically overlap with river centerlines. This overlap may cause misclassification of lentic environments as lotic. As a result, our estimates of lentification are likely conservative. Similarly, to limit misclassification in heavily mined landscapes with substantial connectivity between mining ponds and the river channel, cumulative cost mapping was limited to within 1500 m of the GRWL centerlines. Thus, some small gaps in the river channel mask exist where the river has moved laterally further than 1500 m from the historic centerline. As a final step, small gaps in the river channel mask along narrow river segments at the edge of satellite detectability were filled by dilating and then eroding the river channel mask by two Landsat pixels (60 m). All surface waters outside of the river channel mask were considered lentic. Trends in annual changes in surface water extent for both lentic and lotic systems were calculated on a watershed basis using linear regression.

Deforestation within the study period was calculated using the Hansen Global Forest Change dataset v1.6 (*40*), which contains 30-m resolution global forest change annually between 2001 and 2018. Since all deforestation mobilizes soil and therefore creates opportunities for Hg transport, reported deforestation includes that caused by all sources (e.g., ASGM, natural river erosion, and development), which potentially reduces the overall signal from deforestation directly linked to mining. Conversion rates to aquatic systems and barren soil were calculated by overlaying the water mask with the deforestation mask lagged by 1 year (i.e., delineated into areas that were water the year following deforestation versus land the year following deforestation). Total areas for both barren and aquatic conversion were then calculated for each watershed within the study area.

Data analyses and statistical analyses

All statistical analyses were performed using R version 3.6.0 statistical software. Statistical tests were performed using an α of 0.05.

Since data were not normally distributed, comparisons were performed using the Kruskal-Wallis analysis of variance on ranks, followed by the Dunn's test for pairwise comparisons. In all figures, we report statistically significant differences between groups ($P < 0.05$) using letters, with groups sharing a letter having no statistically significant difference. Reported mercury concentrations in the manuscript represent the means and SE.

SUPPLEMENTARY MATERIALS

Supplementary material for this article is available at http://advances.sciencemag.org/cgi/content/full/6/48/eabd4953/DC1

REFERENCES AND NOTES

1. UNEP, "Global mercury assessment" (Geneva, 2018); https://www.unenvironment.org/resources/publication/global-mercury-assessment-2018.
2. G. P. Asner, R. Tupayachi, Accelerated losses of protected forests from gold mining in the Peruvian Amazon. *Environ. Res. Lett.* **12**, 094004 (2017).
3. G. P. Asner, W. Llactayo, R. Tupayachi, E. R. Luna, Elevated rates of gold mining in the Amazon revealed through high-resolution monitoring. *Proc. Natl. Acad. Sci. U.S.A.* **110**, 18454–18459 (2013).
4. J. C. Espejo, M. Messinger, F. Román-Dañobeytia, C. Ascorra, L. E. Fernandez, M. Silman, Deforestation and forest degradation due to gold mining in the Peruvian Amazon: A 34-year perspective. *Remote Sens.* **10**, 1903 (2018).
5. F. De Lucia Lobo, M. Costa, E. M. L. de Moraes Novo, K. Telmer, Distribution of artisanal and small-scale gold mining in the Tapajós River basin (Brazilian Amazon) over the past 40 years and relationship with water siltation. *Remote Sens.* **8**, 579 (2016).
6. E. N. Dethier, S. L. Sartain, D. A. Lutz, Heightened levels and seasonal inversion of riverine suspended sediment in a tropical biodiversity hot spot due to artisanal gold mining. *Proc. Natl. Acad. Sci. U.S.A.* **116**, 23936–23941 (2019).
7. J. H. Mol, P. E. Ouboter, Downstream effects of erosion from small-scale gold mining on the instream habitat and fish community of a small neotropical rainforest stream. *Conserv. Biol.* **18**, 201–214 (2004).
8. K. E. Markham, F. Sangermano, Evaluating wildlife vulnerability to mercury pollution from artisanal and small-scale gold mining in Madre de Dios, Peru. *Trop. Conserv. Sci.* **11**, (2018).
9. N. Alvarez-Berríos, M. Campos-Cerqueira, A. Hernández-Serna, C. J. A. Delgado, F. Román-Dañobeytia, T. M. Aide, Impacts of small-scale gold mining on birds and anurans near the Tambopata Natural Reserve, Peru, assessed using passive acoustic monitoring. *Trop. Conserv. Sci.* **9**, 832–851 (2016).
10. M. M. Veiga, P. A. Maxson, L. D. Hylander, Origin and consumption of mercury in small-scale gold mining. *J. Clean. Prod.* **14**, 436–447 (2006).
11. K. H. Telmer, M. M. Veiga, World emissions of mercury from artisanal and small scale gold mining, in *Mercury Fate and Transport in the Global Atmosphere*, R. Mason, N. Pirrone, Eds. (Springer, 2009), pp. 131–172.
12. M. A. Cardo, P. M. Vargas, *Proyecto: Plan Nacional de Accion Sobre Mercurio en el Sector de la Mineria de oro Artesanal y de Pequena Escala en el Peru* (Artisanal Gold Council 2017).
13. C. T. Driscoll, R. P. Mason, H. M. Chan, D. J. Jacob, N. Pirrone, Mercury as a global pollutant: Sources, pathways, and effects. *Environ. Sci. Technol.* **47**, 4967–4983 (2013).
14. A. M. Scheuhammer, M. W. Meyer, M. B. Sandheinrich, M. W. Murray, Effects of environmental methylmercury on the health of wild birds, mammals, and fish. *Ambio* **36**, 12–18 (2007).
15. C. A. Eagles-Smith, E. K. Silbergeld, N. Basu, P. Bustamante, F. Diaz-Barriga, W. A. Hopkins, K. A. Kidd, J. F. Nyland, Modulators of mercury risk to wildlife and humans in the context of rapid global change. *Ambio* **47**, 170–197 (2018).
16. E. Ha, N. Basu, S. Bose-O'Reilly, J. G. Dórea, E. McSorley, M. Sakamoto, H. M. Chan, Current progress on understanding the impact of mercury on human health. *Environ. Res.* **152**, 419–433 (2017).
17. J. F. Sanchez, A. M. Carnero, E. Rivera, L. A. Rosales, G. Christian Baldeviano, J. L. Asencios, K. A. Edgel, J. M. Vinetz, A. G. Lescano, Unstable malaria transmission in the southern Peruvian Amazon and its association with gold mining, Madre de Dios, 2001-2012. *Am. J. Trop. Med. Hyg.* **96**, 304–311 (2017).
18. D. Ferring, H. Hausermann, The political ecology of landscape change, malaria, and cumulative vulnerability in central Ghana's gold mining country. *Ann. Am. Assoc. Geogr.* **109**, 1074–1091 (2019).
19. S. Bose-O'Reilly, R. Schierl, D. Nowak, U. Siebert, J. F. William, F. T. Owi, Y. I. Ir, A preliminary study on health effects in villagers exposed to mercury in a small-scale artisanal gold mining area in Indonesia. *Environ. Res.* **149**, 274–281 (2016).
20. S. E. Diringer, A. J. Berky, M. Marani, E. J. Ortiz, O. Karatum, D. L. Plata, W. K. Pan, H. Hsu-Kim, Deforestation due to artisanal and small-scale gold mining exacerbates soil and mercury mobilization in Madre de Dios, Peru. *Environ. Sci. Technol.* **54**, 286–296 (2020).
21. J. R. Gerson, C. T. Driscoll, H. Hsu-Kim, E. S. Bernhardt, Senegalese artisanal gold mining leads to elevated total mercury and methylmercury concentrations in soils, sediments, and rivers. *Elem. Sci. Anth.* **6**, 11 (2018).
22. S. E. Diringer, B. J. Feingold, E. J. Ortiz, J. A. Gallis, J. M. Araújo-Flores, A. Berky, W. K. Y. Pan, H. Hsu-Kim, River transport of mercury from artisanal and small-scale gold mining and risks for dietary mercury exposure in Madre de Dios, Peru. *Environ Sci Process Impacts* **17**, 478–487 (2015).
23. L. Maurice-Bourgoin, B. Quemerais, P. Moreira-Turcq, P. Seyler, Transport, distribution and speciation of mercury in the Amazon River at the confluence of black and white waters of the Negro and Solimões Rivers. *Hydrol. Process.* **17**, 1405–1417 (2003).
24. K. Biber, S. D. Khan, M. T. Shah, The source and fate of sediment and mercury in Hunza River basin, Northern Areas, Pakistan. *Hydrol. Process.* **29**, 579–587 (2015).
25. M. Moreno-Brush, J. Rydberg, N. Gamboa, I. Storch, H. Biester, Is mercury from small-scale gold mining prevalent in the southeastern Peruvian Amazon? *Environ. Pollut.* **218**, 150–159 (2016).
26. C. M. Cañas, P. R. Waylen, Modelling production of migratory catfish larvae (Pimelodidae) on the basis of regional hydro-climatology features of the Madre de Dios basin in southeastern Peru. *Hydrol. Process.* **26**, 996–1007 (2012).
27. J. A. Fleck, M. Marvin-DiPasquale, C. A. Eagles-Smith, J. T. Ackerman, M. A. Lutz, M. Tate, C. N. Alpers, B. D. Hall, D. P. Krabbenhoft, C. S. Eckley, Mercury and methylmercury in aquatic sediment across western North America. *Sci. Total Environ.* **568**, 727–738 (2016).
28. S. G. Todorova, C. T. Driscoll Jr., D. A. Matthews, S. W. Effler, M. E. Hines, E. A. Henry, Evidence for regulation of monomethyl mercury by nitrate in a seasonally stratified, eutrophic lake. *Environ. Sci. Technol.* **43**, 6572–6578 (2009).
29. D. J. X. Gonzalez, Mercury exposure and risk among women of childbearing age in Madre de Dios, Peru. *Trop. Resour. Bull.* **34**, 16–24 (2015).
30. A. C. Gutleb, C. Schenck, E. Stalb, Giant otter (*Pteronura brasiliensis*) at risk? Total mercury and methylmercury levels in fish and otter scats, Peru. *Ambio* **26**, 511–514 (1997).
31. A. García-Sánchez, F. Contreras, M. Adams, F. Santos, Atmospheric mercury emissions from polluted gold mining areas (Venezuela). *Environ. Geochem. Health* **28**, 529–540 (2006).
32. D. E. Bruno, D. A. Ruban, G. Tiess, N. Pirrone, P. Perrotta, A. V. Mikhailenko, V. A. Ermolaev, N. N. Yashalova, Artisanal and small-scale gold mining, meandering tropical rivers, and geological heritage: Evidence from Brazil and Indonesia. *Sci. Total Environ.* **715**, 136907 (2020).
33. K. M. Munson, D. Babi, C. H. Lamborg, Determination of monomethylmercury from seawater with ascorbic acid-assisted direct ethylation. *Limnol. Oceanogr. Methods* **12**, 1–9 (2014).
34. H. Hintelmann, R. D. Evans, Application of stable isotopes in environmental tracer studies – Measurement of monomethylmercury (CH3Hg+) by isotope dilution ICP-MS and detection of species transformation. *Fresenius J. Anal. Chem.* **358**, 378–385 (1997).
35. N. Imura, E. Sukegawa, S.-K. Pan, K. Nagao, J.-Y. Kim, T. Kwan, T. Ukita, Chemical methylation of inorganic mercury with methylcobalamin, a vitamin B12 analog. *Science* **172**, 1248–1249 (1971).
36. J.-F. Pekel, A. Cottam, N. Gorelick, A. S. Belward, High-resolution mapping of global surface water and its long-term changes. *Nature* **540**, 418–422 (2016).
37. N. Gorelick, M. Hancher, M. Dixon, S. Ilyushchenko, D. Thau, R. Moore, Google Earth Engine: Planetary-scale geospatial analysis for everyone. *Remote Sens. Environ.* **202**, 18–27 (2017).
38. G. H. Allen, T. M. Pavelsky, Global extent of rivers and streams. *Science* **361**, 585–588 (2018).
39. X. Yang, T. M. Pavelsky, G. H. Allen, G. Donchyts, RivWidthCloud: An automated Google Earth Engine algorithm for river width extraction from remotely sensed imagery. *IEEE Geosci. Remote Sens. Lett.* **17**, 217–221 (2020).
40. M. C. Hansen, P. V. Potapov, R. Moore, M. Hancher, S. A. Turubanova, A. Tyukavina, D. Thau, S. V. Stehman, S. J. Goetz, T. R. Loveland, A. Kommareddy, A. Egorov, L. Chini, C. O. Justice, J. R. G. Townshend, High-resolution global maps of 21st-century forest cover change. *Science* **342**, 850–853 (2013).

Acknowledgments: We thank F. P. Soncco, B. H. Rivera, A. Chen, A. Lee, F. Machicao, M. Marchese, C. Huamantupa, and local Peruvian miners and community members for field assistance; H. Hsu-Kim, N. Rivera, F. Koenigsmark, N. Neal-Walthall, and A. Wadle for laboratory assistance; M. Silman for feedback in study design; SERNANP, Ejercito Peruano, and the Policia Nacional del Peru for access to the mining ponds in La Pampa; F. Machicao for assistance in translating the manuscript into Spanish; and four anonymous reviewers for feedback that improved the manuscript. **Funding:** Funding was provided by a Duke Global Health Institute Dissertation Fieldwork Grant, Duke University Bass Connections, Duke University Center for Latin American and Caribbean Studies Tinker Research Travel Grant Award, Duke University Dissertation Research International Travel Award, and Josiah Charles Trent Memorial Foundation Endowment Fund grant. **Author contributions:** J.R.Ge. and S.N.T. contributed equally to the study design, data collection, data analysis, and manuscript

preparation. First author order was determined by a coin flip. E.S.B., T.M.P., J.R.Ga., L.E.F., and C.M.V. contributed to the study design and manuscript feedback. X.Y. contributed to the remote sensing analysis and manuscript feedback. **Competing interests:** The authors declare that they have no competing interests. **Data and materials availability:** A Spanish translation of this manuscript can be found in Supplementary Materials. All code for used within this analysis can be found at https://github.com/SimonTopp/MadreDeDios. Basin scale hydroscape visualization can be accessed at https://sntopp.users.earthengine.app/view/mdd-hydroscape-explorer. Chemical data from all water bodies can also be found in table S1.

Submitted 24 June 2020
Accepted 14 October 2020
Published 27 November 2020
10.1126/sciadv.abd4953

Citation: J. R. Gerson, S. N. Topp, C. M. Vega, J. R. Gardner, X. Yang, L. E. Fernandez, E. S. Bernhardt, T. M. Pavelsky, Artificial lake expansion amplifies mercury pollution from gold mining. *Sci. Adv.* **6**, eabd4953 (2020).